

# Relation between microstructures of martensite and prior austenite in 12 wt% Cr ferritic steel

Y. Kinoshita · V. A. Yardley · S. Tsurekawa

Received: 31 August 2010/Accepted: 30 December 2010/Published online: 15 January 2011  
© Springer Science+Business Media, LLC 2011

**Abstract** Tempered martensitic 9–12 wt% Cr ferritic steels are used as heat resistant materials in power plant, where service under conditions of high temperature and pressure for several decades is required, and an adequate resistance to creep is one of the key requirements. In this type of steels, failure has been found to occur preferentially at prior austenite grain boundaries if the prior austenite grains are coarse. It appears that the prior austenite grain boundaries can act as a site of especial weakness in the tempered martensitic microstructure. It would therefore be useful to investigate whether the properties of prior austenite grain boundaries could be modified by some appropriate thermomechanical processing method. One approach to this is to attempt to increase the fraction of annealing twins in the austenite phase and to investigate whether this has an effect on the properties of the martensite after transformation and tempering. In this study, thermomechanical treatments involving hot-rolling have been applied and the fraction of austenite twins produced determined using electron back-scatter diffraction analysis. The treatment giving the highest fraction of austenite twins was identified and the effect of the increase in twin fraction on the characteristics of the martensite was investigated. It was found that the fraction of coincidence site lattice boundaries in martensite along prior austenite grain boundaries increased with increasing fraction of prior austenite twin boundaries.

## Introduction

Recent environmental concerns are a strong driving force for the development of new power plant materials to withstand higher operating temperatures in order to increase thermal efficiency. 9–12 wt% Cr ferritic steels with tempered martensite microstructures have been developed as heat-resistant materials for boilers, turbines and pipework, in which the operating temperature is 723–893 K (450–620 °C) [1] and a service life of several decades is required. Under such conditions, one major failure mode is creep fracture. In previous studies of tempered martensite ferritic steels with other chemical compositions, it was reported that creep fracture preferentially occurred along prior austenite grain boundaries when the prior austenite grains were coarse [2, 3]. Electron backscatter diffraction investigations in the immediate vicinity of creep cracks in 9–12 wt% Cr steels by one of the present authors also indicates preferential nucleation of voids at prior austenite grain boundaries [4]. Possible reasons for this are that prior austenite grain boundaries act as preferential sites for the precipitation of coarse carbides that can act as void nucleation sites [5–9], and that the recovery of the high density of dislocations promotes the formation of coarse subgrains near prior austenite grain boundaries [6]. In addition, the observed brittle fracture at prior austenite grain boundaries in 12% Cr steels may be due to the preferential segregation of phosphorus to prior austenite grain boundaries [10]. If it were possible to control the properties of prior austenite grain boundaries such that these phenomena occurred to a lesser extent, then it may be possible to increase the resistance of these types of microstructure to creep. There has so far been very little previous work on applying grain boundary engineering methods to ferritic heat-resistant steels, probably because of the relative difficulty of introducing coincidence site lattice boundaries into materials

Y. Kinoshita · V. A. Yardley · S. Tsurekawa (✉)  
Department of Materials Science and Engineering, Graduate  
School of Science and Technology, Kumamoto University,  
Kumamoto 860-8555, Japan  
e-mail: turekawa@kumamoto-u.ac.jp

V. A. Yardley  
Institut fuer Werkstoffe, Ruhr-Universitaet Bochum,  
44780 Bochum, Germany

with body-centered cubic structures compared to that in face-centered cubic materials. Gupta et al. [11] used a thermo-mechanical processing route consisting of cold-rolling at a reduction ratio of 5%, annealing at 1323 K (1050 °C—in the austenite phase field for this steel) for 1 h, air cooling and tempering at 1073 K (800 °C) for 0.66 h to manipulate the grain boundary character distribution in the 9 wt% Cr steel T91. This processing route was found to increase the CSL boundary fraction to 0.36,<sup>1</sup> which was larger than that of a conventionally processed sample (0.28). Subsequently, Was et al. [12] demonstrated that the creep rate of T91 processed by this route was lower than that of standard T91. Since the high-temperature austenite phase of this material is face-centered cubic (fcc), it is expected that it will be relatively easy to introduce  $\Sigma 3$  twins and related coincidence site lattice boundaries ( $\Sigma 9$  and  $\Sigma 27$ ) by deformation and annealing, as has already been successfully accomplished in SUS 304 austenitic steels [13]. In this study, it was investigate the optimum thermomechanical processing route to increase the fraction of  $\Sigma 3$  and related boundaries in the austenite phase and the effect of changes in this fraction and in the prior austenite grain size on the grain boundary microstructure of the martensite produced after tempering.

## Experimental

### Specimen and microstructure control

The material used in this study was a commercially processed rotor steel whose chemical composition was 0.09C–10.89Cr–0.17Mo–2.61Nb–0.2 V–2.52Co (wt%) and whose mechanical properties are reported in Ref. [14], where it is referred to as steel No. 1. In order to introduce annealing twins by rolling in the austenite phase, the specimens, 10 mm × 10 mm × 10 mm in size, were first austenitised at 1273 K for 45 min, then hot-rolled to different reduction ratios followed by annealing at 1273 K for 45 min and air-cooling. Previous work on austenitic stainless steels indicates that relatively low rolling ratios (around 5%) before annealing produce the highest fraction of CSL-grain boundaries [13]. In this study, reduction ratios of 5, 10, and 15% were used, and a specimen that was annealed for the same total length of time but not rolled was also produced. In addition, a specimen hot-rolled at a 5% reduction ratio, then annealed at 1273 K for 72 h, was prepared to

determine whether a longer annealing time helped to increase propagation of twins into the bulk, as was reported by Shimada et al. [13]. Specimens were cut normal to the rolling direction to observe microstructure.

### Microstructure observations

#### *Scanning electron microscopy (SEM)*

In order to determine the prior austenite grain size, etched specimens were observed using scanning electron microscopy (SEM). The solution used for etching was a mixture of picral (picric acid 8 g, ethanol 200 ml) 0.9: concentrated hydrochloric acid 0.1, and the etching time was 1.5 min. In order to measure the prior austenite grain size from SEM images, a linear intercept method was used. In this method, more than 50 lines were randomly drawn on all images showing more than 50 prior austenite grains.

#### *Electron backscatter diffraction (EBSD)*

For quantitative evaluation of microstructure, automated SEM/EBSD observations were conducted using a Hitachi FEG-SEM (S-4200) operated using an accelerating voltage of 30 kV and a beam current of 8  $\mu$ A with 0.25  $\mu$ m step size. For EBSD observation, specimens were electro-polished at a voltage of 10 V and a current density of  $0.2 \times 10^{-2}$  A/mm<sup>2</sup> using a solution of acetic acid 0.77: perchloric acid 0.23 to give a strain-free surface. Block sizes were determined from the EBSD data using the “TSL OIM analysis 5.2” software supplied with the EBSD system. The misorientation of block interfaces is always greater than 15° in the lath martensite microstructure [15]. The EBSD observation analysis software defines a “grain” as a region bounded by grain boundaries of misorientation  $\geq 15^\circ$ . The blocks in the present martensitic microstructure therefore qualify as grains according to this definition, and measurements of block size could be performed easily. (The length fraction of boundaries with misorientation angles between 15° and 45° was found to be almost zero, so the precise threshold for definition of a “grain” or “block” is in any case relatively unimportant.)

### Determination of prior austenite grain boundary using EBSD

Because martensite microstructures are fine and complex, it is often difficult to determine the position of prior austenite twin boundaries by optical examination of the resulting martensite. However, the crystallographic characteristics of martensite allow EBSD/OIM analysis to be used to determine whether twins were present in the prior austenite microstructure and to determine the positions of the prior

<sup>1</sup> Tempered martensite ferritic steels have a complex substructure within each prior austenite grain (PAG), consisting of packets, which are further subdivided into blocks; blocks also contain sub-blocks. The block and sub-block boundaries are classified as high and low angle boundaries, respectively. However, it is unclear from Gupta’s paper which boundaries (PAGB, block boundary and sub-block boundary) they included to evaluate the CSL boundary fraction.

austenite grain and twin boundaries. In relatively low-carbon steels such as the material under consideration here, the Kurdjumov–Sachs (K–S) orientation relationship is a good approximation, although not a perfect description, of the orientation relationship between martensite and austenite [16, 17]. Considering only the rotational component of the transformation from austenite to martensite a position vector  $\mathbf{x}^{(A)}$  in austenite is transformed to one of the  $i$  possible martensitic orientation variants the  $\mathbf{x}_i^{(M)}$  by the transformation matrices  $\mathbf{T}_i$ .

$$\mathbf{x}_i^{(M)} = \mathbf{T}_i \mathbf{x}^{(A)} \quad (1)$$

Here,  $i$  is an integer which for the K–S relationship lies between 1 and 24. Twinning on the {111} plane in fcc can be expressed as a rotational operation  $\mathbf{T}_T$  corresponding to a  $60^\circ<111>$  misorientation. If a twin is formed in the austenite phase, the orientation relationship between the twin and the parent austenite can be expressed as

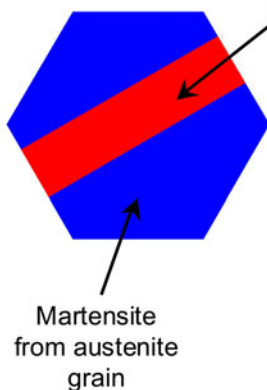
$$\mathbf{x}_T^{(A)} = \mathbf{T}_T \mathbf{x}^{(A)} \quad (2)$$

where  $\mathbf{x}_T^{(A)}$  represent the position vector in the twin. The orientations of the martensite variants from a twinned prior austenite grain are given, with respect to the orientation of the parent austenite, by:

$$\mathbf{x}_T^{(M)} = \mathbf{T}_T \mathbf{x}_T^{(A)} = (\mathbf{T}_i \mathbf{T}_T) \mathbf{x}^{(A)} \quad (3)$$

Figure 1 represents a calculated pole figure of martensite variants from a parent austenite grain and twin-related martensite variants referred to the  $\langle 001 \rangle \gamma$  axes of the parent, assuming the K–S orientation. In this pole figure, the variants from the parent are displayed in blue and those from the twin in red. These variants produce a characteristic “key-hole”-type appearance on the pole figure and 1/4 of the variants from the twinned grains share poles with variants from the parent austenite grain.

**Fig. 1** Calculated pole figure showing the {100} poles of martensite variants from a parent and one  $60^\circ<111>$  twin in austenite with respect to the  $\langle 001 \rangle \gamma$  axes of the parent, assuming the K–S orientation relation



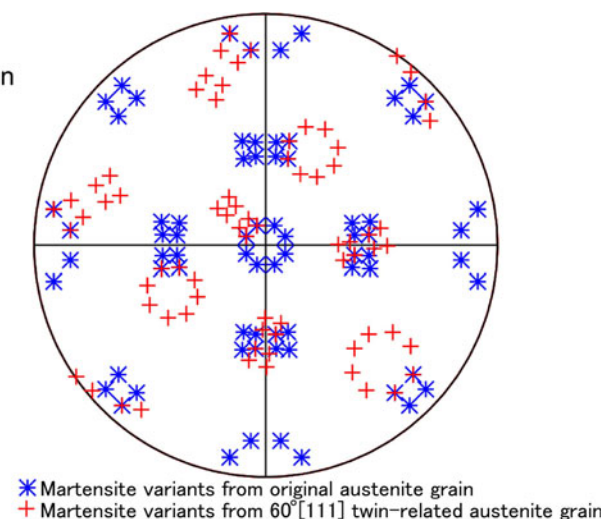
Although the K–S relationship is not an exact description of the orientation relationship in this material and variations in orientation within austenite grains may also, in practice, produce scatter, the calculated pole figure is sufficiently similar to what is observed in practice in EBSD for us to be able to use it to identify the presence of twins in prior austenite.

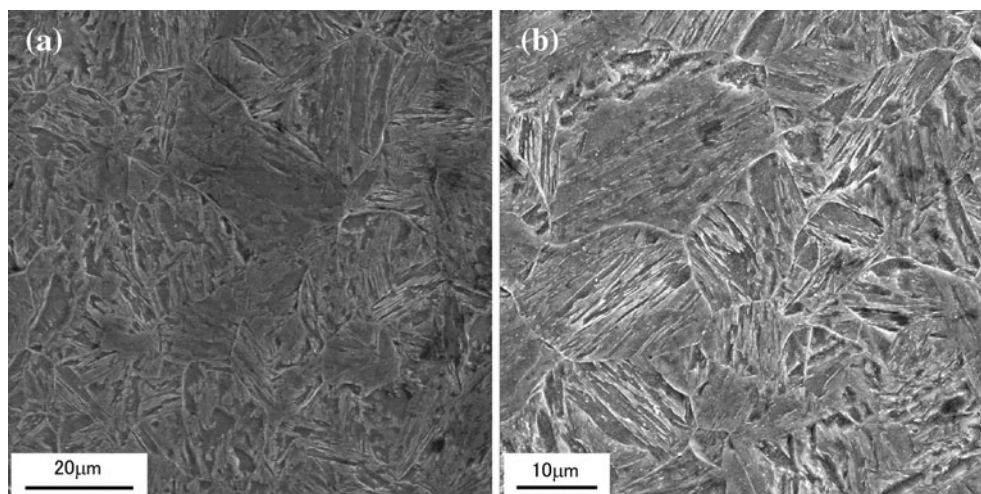
## Results and discussion

### Microstructural characterization

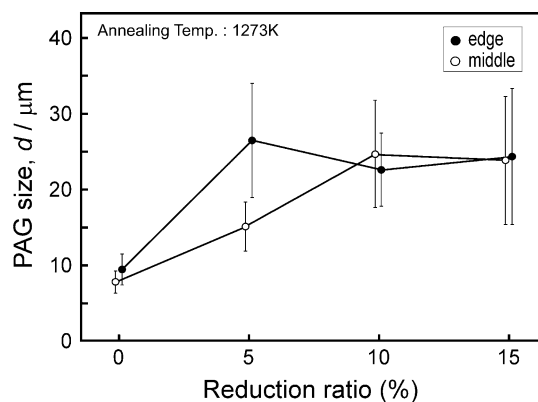
#### Prior austenite grain size

Figure 2 shows SEM images of the specimen that was hot-rolled at 1273 K at 5% reduction ratio and subsequently annealed at 1273 K for 45 min. These images confirm the formation of a typical lath martensitic microstructure, with several prior austenite grain boundaries visible. The average prior austenite grain diameter was determined in different two areas, one just beneath the surface (hereafter denoted as ‘edge’) and the other at the center of the sample (hereafter denoted as ‘middle’). The average prior austenite grain diameter measured is plotted against the reduction ratio in Fig. 3. The prior austenite grain diameter of the specimen without rolling (0%) was less than 10  $\mu\text{m}$  in both edge and middle areas. The average prior austenite grain diameter in the edge area of the specimen rolled to 5% was found to be the largest among those measured. The strain introduced by 5% rolling appeared to strongly promote grain boundary migration. On the other hand, a higher strain than that given by the 5% reduction ratio may have cause recrystallization instead of grain growth, resulting in the observed smaller grain size. In the case of the 5% reduction ratio, an annealing time of 45 min did not appear





**Fig. 2** SEM micrographs showing prior austenite-grain boundaries in lath martensite of a 12Cr steel that was hot-rolled at 1273 K at 5% reduction ratio and subsequently annealed at 1273 K for 45 min: **a** edge and **b** middle



**Fig. 3** Relation between the average prior austenite grain size and reduction ratio

to be long enough for grain growth into the middle area, since the prior austenite grains at the edge were larger than those in the middle. However, annealing for 72 h gave a homogeneous grain diameter of approximately 40 μm in both the edge and the middle regions, as shown in Fig. 4.

#### Block size

The relationship between reduction ratio and block size is shown in Fig. 5. The “block size” parameter  $\bar{v}$  for a sample is found from an area-weighted average given by:

$$\bar{v} = \frac{\sum_{i=1}^N A_i v_i}{\sum_{i=1}^N A_i} \quad (4)$$

where  $A_i$  is the area of grain  $i$  and  $v_i$  is the value of the block size for grain  $i$ . It is found that the variation of the block size with the reduction ratio shows a similar trend to that of prior austenite grain diameter. The average block size increased with increasing annealing time, and the

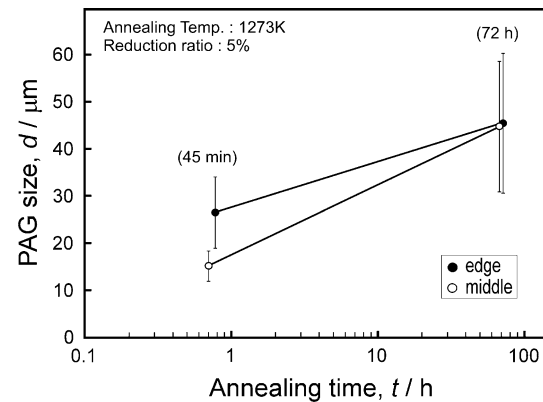


**Fig. 4** Changes in the average prior austenite grain size with annealing time at 1273 K for the specimen hot-rolled to 5% at 1273 K

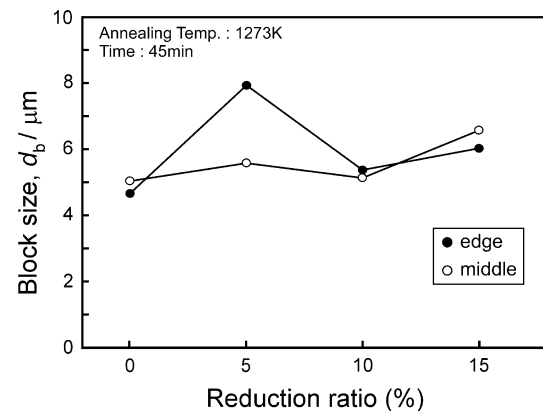


**Fig. 5** Relation between the average block size and reduction ratio for the specimen hot-rolled at 1273 K and subsequently annealed at 1273 K for 45 min

longer annealing time, the smaller the difference between the block sizes at the edge region and those in the middle region, as shown in Fig. 6. Figure 7 shows the relationship

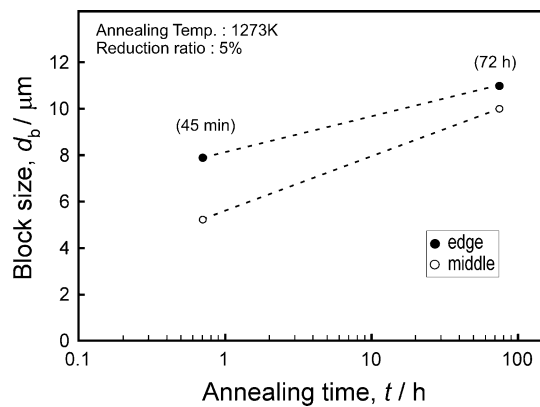


**Fig. 6** The average block size as a function of annealing time for the specimen hot-rolled at 5% reduction ratio and annealed at 1273 K

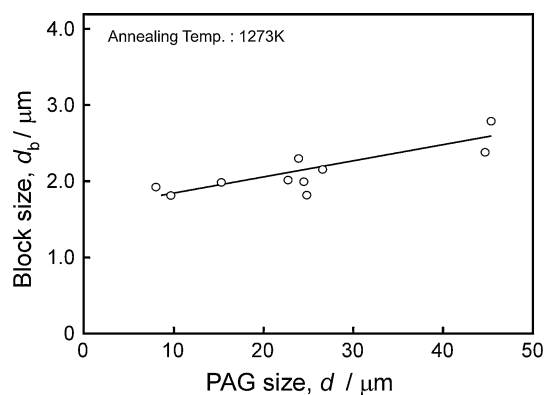


**Fig. 7** Correlation between the average block size and the average prior austenite grain size

between the block size and the size of prior austenite grain diameter; the block size shows a clear linear positive correlation with prior austenite grain diameter. This agrees with previous results, measured using a slightly different technique, in the same steel [18].

#### Crystallographic analysis

Figure 8 describes the experimental identification of twins induced in austenite phase. Figure 8a, b are an inverse pole figure (IPF) map and a pole figure for the martensite phase in the 12Cr steel, respectively. It is not easy to recognize the position of prior austenite grain boundaries and twin boundaries by eye in the map. When a possible prior austenite grain area consisting of several martensite variants in this IPF map is highlighted using the TSL OIM Analysis 5 software as demonstrated in Fig. 8c, the poles arising from these variants appear in the same color on the pole figure (Fig. 8d). If the pattern made by the highlighted poles on the pole figure is consistent with the theoretically

calculated pattern shown in Fig. 1, then prior austenite twin boundaries must have been present at the positions between the areas highlighted in red and blue (Fig. 8c). Using these procedures, the authors can find the twin-related austenite grains in inverse pole figure (IPF) maps even when no retained austenite is present. Annealing twin boundaries are typically very straight-sided. However, twin boundaries identified using our method often have irregular-shaped interfaces. This is because at coherent  $\Sigma 3$  twin boundaries in austenite, the martensite variants formed are often the variants “shared” between the twin-related austenite grain and the parent austenite grain, giving a continuous packet across the prior austenite twin boundary. Therefore, it is difficult to determine precisely the position of the twin boundary, and experimentally identified twin boundaries can have an irregular-shaped interface.

Figure 9 shows IPF maps for the specimen that was hot-rolled at 1273 K with 5% reduction ratio and subsequently annealed at 1273 K for 45 min. Figure 9a displays the character of individual grain boundaries and Fig. 9b shows the prior austenite grain boundaries and the interfaces of  $\Sigma 3^n$  twin-related boundaries in the grain. The terminology  $\Sigma 3^n$  is used because when two twin boundaries meet at a triple junction, the third grain boundary must also be a special,  $\Sigma 3^n$  boundary from the  $\Sigma$  production rule. In Fig. 9b, general prior austenite grain boundaries are delineated in black, prior austenite  $\Sigma 3$  boundaries (twin boundaries) in red and prior austenite  $\Sigma 3^n$  boundary other in white. It appears that the larger the prior austenite grain, the more twins were found within the grains. This is consistent with a process of grain growth (grain boundary migration) is accompanied by twin formation.

#### Quantitative analysis of grain boundary microstructure

##### Fraction of $\Sigma 3^n$ grain boundaries in austenite

From the results of the analysis described above, the fraction of  $\Sigma 3^n$  grain boundaries in the austenite phase at 1273 K was evaluated from:

$$f_{(\Sigma 3^n)}^{(\gamma)} = \frac{L_{(\Sigma 3^n)}^{(\gamma)}}{L_{(\text{total})}^{(\gamma)}}, \quad (5)$$

where  $L_{(\Sigma 3^n)}^{(\gamma)}$  is the total length of  $\Sigma 3^n$  grain boundaries in austenite, and  $L_{(\text{total})}^{(\gamma)}$  the total length of all grain boundaries in austenite. Figure 10 shows the fraction of  $\Sigma 3^n$  grain boundaries in austenite  $f_{(\Sigma 3^n)}^{(\gamma)}$  as a function of the reduction ratio for the specimens hot-rolled at 1273 K and subsequently annealed at 1273 K for 45 min. The prior austenite grain boundary length was measured both at the edge and

**Fig. 8** Experimental identification of twins induced in austenite phase. **a** and **b** are an inverse pole figure (IPF) map and a pole figure for the martensite phase in the 12Cr steel, respectively. **c** represents a possible prior austenite grain area consisting of several martensite variants highlighted using the OIM software in the selected area shown in **a** with dashed line, and the poles arising from these variants appear in a common color on the pole figure shown in **d**

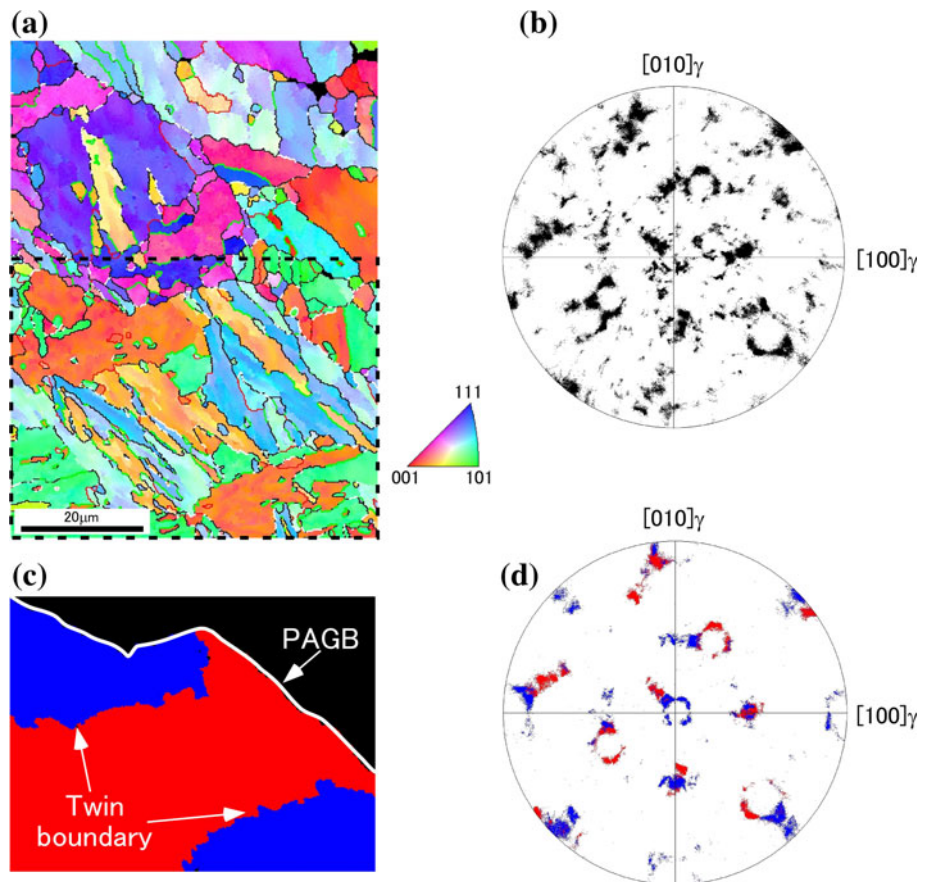
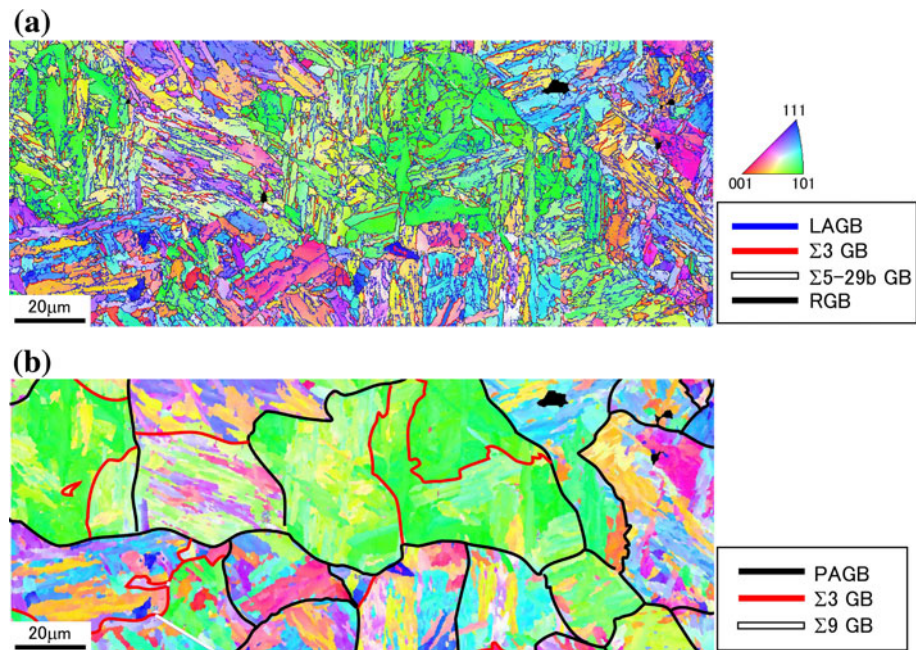


**Fig. 9** IPF maps for the specimen hot-rolled at 1273 K at 5% reduction ratio and subsequently annealed at 1273 K for 45 min. **a** shows the character of individual grain boundaries and **b** the prior austenite grain boundaries and the prior  $\Sigma 3^n$  boundaries determined



in the middle of the specimen, and then  $f_{(\Sigma 3^n)}^{(\gamma)}$  was calculated. It was found that  $f_{(\Sigma 3^n)}^{(\gamma)}$  represented more than 0.3 of the total length of prior austenite grain boundaries even in

the specimen without rolling demonstrating the relatively high propensity to twinning in austenite even without any special. With a 5% reduction ratio, this fraction in the edge area differed little from that without rolling. However, the

fraction of  $\Sigma 3^n$  grain boundaries increased up to approximately 0.5 in the middle area. At higher reduction ratios, this fraction decreased again. This finding is consistent with the results reported by Shimada et al. [13], who found a peak in the fraction of CSL (mainly  $\Sigma 3$ ) boundaries at a 5% reduction ratio for austenitic stainless steel (SUS304). A higher strain than this is likely to promote recrystallization rather than grain boundary migration, and to introduce new random boundaries. Recrystallization is particularly likely to occur in the edge area closest to the applied load. The fraction at 15% reduction ratio is considerably lower in the edge area than that in the middle. A small strain given by a reduction ratio of around 5% most probably enables annealing twins to be formed by migrating grain boundaries. Figure 11 shows the changes in the fraction of  $\Sigma 3^n$  grain boundaries in the austenite phase at 1273 K with the annealing time after hot-rolling at 1273 K at the reduction ratio of 5%. The fraction slightly increased with increasing annealing time. The increase in

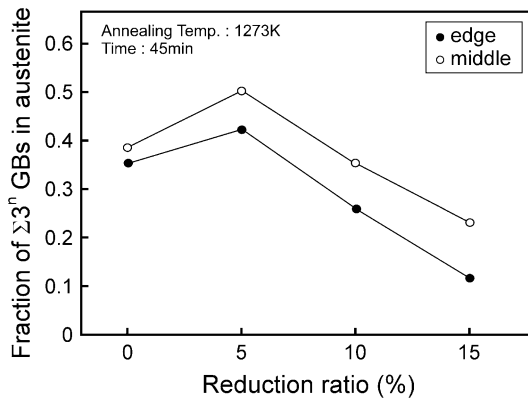


**Fig. 10** The fraction of  $\Sigma 3^n$  GB in austenite  $f_{(\Sigma 3^n)}^{(7)}$  as a function of the reduction ratio for the specimens hot-rolled at 1273 K and subsequently annealed at 1273 K for 45 min

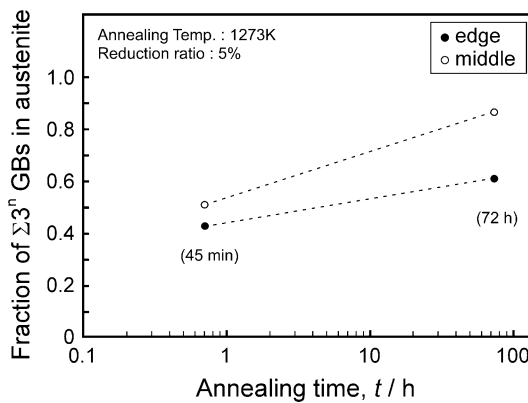


**Fig. 11** Changes in the fraction of  $\Sigma 3^n$  GB in the austenite phase at 1273 K with the annealing time after hot-rolling at 1273 K at the reduction ratio of 5%

the fraction with annealing time was more significant in the middle area than in the edge area. The fraction reached 0.9 in the middle area for 72 h annealing.

Recent in situ SEM/EBSD observations have found that grain boundary migration is often accompanied by twin formation in nanocrystalline Ni [19] and in Fe–Ni [20]. Figure 12 shows the relationship between the fraction of  $\Sigma 3^n$  grain boundaries in the austenite phase and the prior austenite grain diameter. The fraction of  $\Sigma 3^n$  grain boundary has a positive correlation with increasing prior austenite grain size, although data scatter is relatively large. Therefore, it is believed that annealing twins are introduced during grain growth in the austenite phase.

#### Relation between grain boundary character distribution in martensite and the fraction of $\Sigma 3^n$ grain boundary in the austenite

Figure 13 represents the relation between grain boundary character distribution in martensite and the fraction of  $\Sigma 3^n$  grain boundaries in the austenite. Here, all grain boundaries with misorientation  $>2^\circ$  are included in this. The fraction of

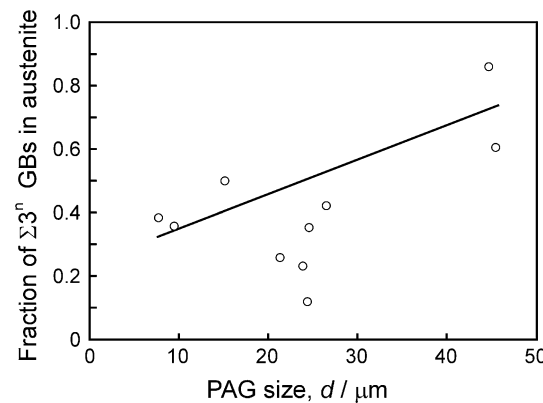


**Fig. 12** Relation between the fraction of  $\Sigma 3^n$  GB in the austenite phase and the prior austenite grain (PAG) size in martensite

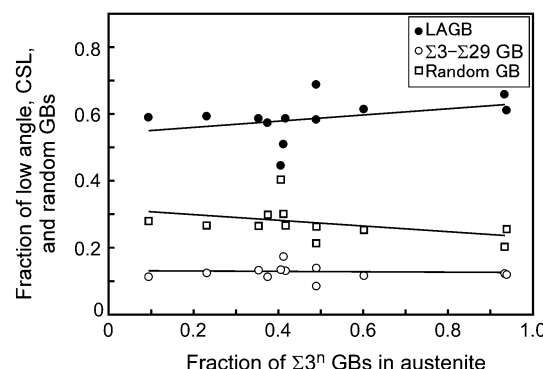


**Fig. 13** Relation between the grain boundary character distribution (GBCD) in martensite and the fraction of  $\Sigma 3^n$  GB in the austenite

low-angle grain boundaries, most of which probably arise from the sub-block boundaries [15] within martensitic blocks, is found to increase slightly with increasing fraction of  $\Sigma 3^n$  prior austenite grain boundaries, whereas that of random grain boundaries decreases. On the other hand, the fraction of CSL-grain boundaries in martensite is less dependent on the fraction of  $\Sigma 3^n$  grain boundaries in austenite.

#### Fraction of martensite CSL grain boundaries along prior austenite grain boundaries

The relationship between the grain boundary microstructure in martensite and that in austenite prior to transformation was examined. As described in the introduction, prior austenite grain boundaries in ferritic steels with tempered martensitic microstructures appear to have a higher susceptibility to initiation of damage than do prior austenite grain interiors. Thus, the authors are particularly interested in the grain boundary character distribution of martensite along prior austenite grain boundaries. Figure 14 is a plot of the fraction of martensite CSL-grain boundaries along prior austenite-grain boundaries (PAGB), excluding prior austenite twin boundaries  $f_{(\text{CSL})}^{\text{PAGB}}$  and the fraction of  $\Sigma 3^n$  grain boundary in austenite prior to transformation. Of particular importance is the finding that the fraction of CSL-grain boundaries on the prior austenite-grain boundaries increases as a function of the fraction of  $\Sigma 3^n$  grain boundaries in the austenite phase. The value of  $f_{(\text{CSL})}^{\text{PAGB}}$  has a maximum of approximately 0.27, which is as about the same as the fractions of CSL boundaries in thermomechanically processed materials with bcc structure (around 20–40%) [21]. For comparison, it was measured the fraction of CSL boundaries in a commercially produced 12 wt% Cr steel (Austenitisation temperature: 1323 K, Quench: oil, Tempering temperature: 993 K, Cooling: air cooling), and found it to be approximately 0.17. Therefore, it appears that the application of twin-assisted grain boundary engineering to austenite at elevated temperatures prior to martensite transformation is useful for increasing the fraction of CSL boundaries on the prior austenite-grain boundaries in tempered martensite ferritic steels. The mechanism by which this occurs is not clear at present. The introduction of twins can transform adjoining sections of random grain boundaries into CSL boundaries by the  $\Sigma$  production rule; for example, a  $\Sigma 51$  grain boundary (customarily classed as random) can transform, where it intersects a  $\Sigma 3$  twin, to a  $\Sigma 17$  boundary. However, the relationship between misorientation and CSL character of austenite grain boundaries and the production of CSL-related martensite variants is not an obvious one. It is likely that there are some misorientations in austenite that give

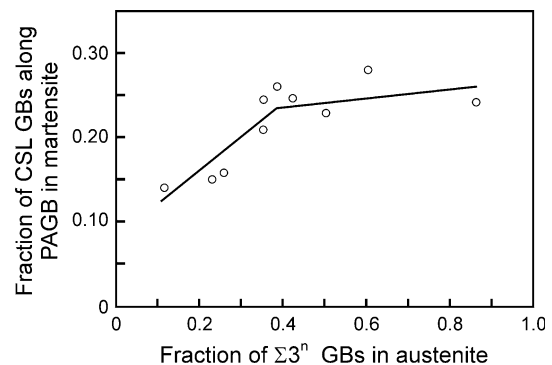


**Fig. 14** The fraction of CSL GBs along the prior austenite grain boundaries (PAGB) in martensite as a function of the fraction of  $\Sigma 3^n$  GBs in austenite

rise to a particularly high fraction of CSL-related martensite variants (in addition to the formation of “shared” martensite variants at  $\Sigma 3$  austenite boundaries), and it could be that when CSL-related variants are possible then they are preferentially selected over non-CSL-related variants. However, a full investigation of this would require calculation of all combinations of martensite variants for all possible misorientations in austenite, and this is beyond the scope of this article.

The increase in prior austenite twin and twin-related boundary fraction and in the fraction of CSL-related grain boundary misorientations in martensite along prior austenite-grain boundaries may be indicative of an increase in what could loosely be termed “microstructural coherency” at sites that have been identified as particularly susceptible to the initiation of damage. Creep tests are planned to determine whether these microstructural changes are associated with an increase in creep resistance.

#### Conclusions

A thermomechanical processing route using hot-rolling and subsequent annealing for introducing a high fraction of twin boundaries into the austenite phase of tempered martensite ferritic steels has been developed. The relationship between the grain boundary microstructure in austenite prior to martensite transformation and that in martensite was studied. The main results obtained are as follows:

1. Among the thermomechanical treatments at 1273 K for 45 min, hot-rolling at a reduction ratio of 5% introduced the maximum fraction of twin and twin-related boundaries (0.49). This is consistent with previous findings in fcc materials, where a relatively low reduction ratio promotes grain growth accompanied by twin formation, and higher rolling ratios instead promote recrystallization.

2. In the sample with rolling ratio 5%, a post-roll annealing time of 45 min at 1273 K resulted in differences in grain size and  $\Sigma 3^n$  boundary fraction between the outer surface and the bulk. However, increasing the annealing time to 72 h gave a fraction of  $\Sigma 3^n$  boundaries in austenite of around 0.9 even in the bulk. An annealing time of 72 h was clearly sufficient for grain growth and accompanying formation of prior austenite twins throughout the thickness in specimens of this size. Clearly the post-roll annealing time required will depend on the sample size.
3. The fraction of CSL boundaries along prior austenite grain boundaries increased with increasing fraction of  $\Sigma 3^n$  prior austenite grain boundaries and the highest value (0.27) was given by a long annealing treatment (72 h) after rolling at a reduction of 5%. This result helps to support the idea that microstructural control in the austenite phase could be effective in controlling the grain boundary character distribution in the martensitic microstructure.

**Acknowledgements** The authors wish to express their sincere thanks to Associate Professor Y. Morizono for useful discussions. YK is grateful to Dr. T. Yamamuro for his help with experimental study. This study was supported by an ISIJ (The Iron and Steel Institute of Japan) Research Promotion Grant.

## References

1. Otsuka T, Kaneko M (2007) In: Cen K, Chi Y, Wang F (eds) Challenges of power engineering and environment, vol 1. Springer, New York, p 214
2. Hong SH, Yu J (1989) Scripta metall 23:1057
3. Kimura K, Ohi N, Shimazu K, Matsuo T, Tanaka R, Kikuchi M (1987) Scripta metall 21:19
4. Yardley VA, Matsuzaki T, Sugiura R, Yokobori AT Jr, Tsurekawa S, Hasegawa Y (2010) J Phys: Conf Ser 240: 012076
5. Brooks CR, Bogni F (1997) Mater Charac 38:103
6. Matsui M, Tabuchi M, Watanabe T, Kubo K, Kinugawa J, Abe F (2001) ISIJ Intern 41:S126
7. Abe F, Horiuchi T, Taneike M, Sawada K (2004) Mat Sci Eng. A 378:299
8. Abe F (2008) Sci Technol Adv Mater 9:013002
9. Abe F (2009) Mat Sci Eng 510–511:64
10. Choudhury A, Padgett RA, Brooks CR (1990) Scripta metal mater 24:1593
11. Gupta G, Alexandreanu B, Was G (2004) Metall Mater Trans A 35A:717
12. Was G, Alexandreanu B, Andresen P, Kumar M (2004) Mat Res Soc Symp Proc 819:N.2.1.1
13. Shimada M, Kokawa H, Wang ZJ, Sato YS, Karibe I (2002) Acta Mater 50:2331
14. Sugiura R, Yokobori AT Jr, Takamori S, Tabuchi M, Fuji A, Yoda M, Kobayashi K, Yokobori T (2006) J Jpn Inst Met 70:452
15. Morito S, Tanaka H, Konishi R, Furuhara T, Maki T (2003) Acta Mater 51:1789
16. Morito S, Yoshida H, Maki T, Huang X (2006) Mat Sci Eng 438–440:237
17. Kitahara H, Ueji R, Tsuji N, Minamino Y (2006) Acta Mater 54:1279
18. Yardley VA, Sugiura R, Matsuzaki T, Tsurekawa S, Yokobori AT Jr, Hasegawa Y (2007) Strength Fract Complex 5:39
19. Tsurekawa S, Fukino T, Matsuzaki T (2009) Int J Mat Res 100:800
20. Fukino T, Tsurekawa S (2008) Mater Trans 49:2770
21. Watanabe T (1993) Text Micro 23:195